Perfluorocyclobutane (PFC-318, *c*-C_4F_8) in the global atmosphere

Mühle et al., 2019

Supplemental text, figures, and tables

AGAGE in situ data are available at

http://agage.mit.edu/data

http://cdiac.ess-dive.lbl.gov/ndps/alegage.html

CSIRO and Bristol inversion results, firn data, etc. are given in

Muhle et al. c-C4F8 2019 Supplemental tables.xlsx

Details on data quality assurance for the measurements of archived air samples of the extra-tropical Southern Hemisphere (SH, Cape Grim Air Archive, CGAA) and extra-tropical Northern Hemisphere (NH)

To reconstruct the atmospheric history of *c*-C_4F_8 in the extra-tropical SH, 41 unique CGAA samples (collected 1978–2009, Langenfelds et al., 2014) were measured at CSIRO in 2011 (Ivy et al., 2012). Three CGAA tanks were measured at the beginning, in the middle, and towards the end of the measurements at CSIRO, with agreements within typical precisions or better (0.01–0.02 ppt). In addition, 8 SH samples were measured at SIO which were sub-sampled from CGAA parent tanks (fill dates 1986–2008, 0.60–1.17 ppt) into evacuated stainless steel (SS) tanks (4.5 L, Essex Industries, USA) with a vacuum manifold and pressure regulator shown not to produce any *c*-C_4F_8 artefacts. They were measured at SIO on Medusa 7 to take advantage of the more sensitive MSD and to evaluate the agreement with Medusa 9 measurements at CSIRO. Four of these CGAA subsamples measured at SIO agreed within precisions (delta mole fractions, Δx = 0.00–0.01 ppt, ratio = 1.0047, R^2 = 0.9994) with their CGAA parents measured at CSIRO, 2 subsamples showed a larger differences (0.018 and 0.027 ppt). The measurements of the seventh subsample and its CGAA parent were rejected, perhaps due to problems during the subsampling or with the parent tank. While we did not measure the CGAA parent of the eighth subsample at CSIRO, we found agreement (Δx = 0.01 ppt) with another CGAA tank of similar air age (Δt = 63 days) measured at CSIRO. Four additional SH samples (fill dates 1995–2010, 0.84–1.25 ppt) were measured at SIO. Three were also in very good agreement with CGAA samples of similar fill date measured at CSIRO (Δx < 0.006 ppt, Δt = 7–23 days) and one showed a larger difference (Δx = 0.05 ppt).

To reconstruct the atmospheric history in the extra-tropical NH, 126 unique air samples mostly filled at SIO and THD (1973–2016) were measured at SIO. Additionally, 3 NH samples (filled in 1980 and 1999) were measured at CSIRO. Two of these tanks measured at CSIRO were filled together at SIO in 1999 with 2 tanks measured at SIO and the agreement is excellent (Δx = <0.007 ppt). The third tank, filled in 1980 at Cape Meares, Oregon, agreed within 0.034 ppt with another NH tank (filled at SIO within 9 days) measured at SIO. Despite this larger difference,

the overall good agreement of NH and SH samples measured at SIO and CSIRO shows that measurements on the involved instruments were comparable and that calibration scales were properly propagated.

Details on bottom-up emission inventories (UNFCCC, EDGAR, NIRs, WSC) for *c*-C_4F_8

Amongst the countries reporting to the United Nations Framework Convention on Climate Change (UNFCCC) (2016), a few countries report *c*-C_4F_8 emissions, most notably France, the USA, and Russia, and the global total ranges from 7 (1993) to 26 (2011) t yr^{-1} (0.007–0.026 Gg yr^{-1}, 1 t = 1 metric ton = 1 tonne = 0.001 Gg). Several countries also or exclusively report emissions of an unspecified mix of PFCs as a sum of CO_2-equivalent (CO_2-eq.) emissions (using global warming potentials, GWP), which may contain *c*-C_4F_8 emissions, most notably Japan (3,260 (2013) – 19,900 (1997) Gg CO_2-eq.), followed by much smaller amounts from France (~139 (2000) – 518 (2012) Gg CO_2-eq.) and a few other European countries.

Based on the National Inventory Report (NIR) for France, their reported emissions of unspecified mix of PFCs, all from category 2G2 (SF_6 and PFCs from other product use), does not contain any *c*-C_4F_8.

Based on the NIR for the Netherlands and Austria, category 2E1 (integrated circuit (IC) or semiconductor (SC) production) could contribute a few to a few ten t yr^{-1} of *c*-C_4F_8 per country if all emissions of unspecified mix of PFCs were *c*-C_4F_8, which is very unlikely. More likely seems that the GWP weighted mix of fugitive emissions from category 2E1 from these countries is similar to the mix for category 2E1 from European countries which report individual emissions for category 2E1. For the European Union, *c*-C_4F_8 represents ~0–8 % of the GWP weighted PFC mix (CF_4, C_2F_6, C_3F_8, *c*-C_4F_8) from 2E1. If the Netherlands and Austria emit 8 % of GWP weighted mix of PFCs in category 2E1 as *c*-C_4F_8, this would sum up to at most a few t yr^{-1}.

The United Kingdom NIR details that their unspecified PFC mix emissions are all from category 2B9 (fluorochemical production) and refers to the UK environmental agency's pollution inventory (https://data.gov.uk/dataset/pollution-inventory). Judging from this inventory and our knowledge of the listed PFC sources, they most likely do not emit any *c*-C_4F_8 and thus category 2B9 does not contain any *c*-C_4F_8 emissions for the UK.

The Japanese NIR details that their emissions of unspecified mix of PFCs stems from categories 2B9, 2E (SC, liquid crystals, and photovoltaic production), and 2F5 (solvents use). For Japan, category 2F5 is comprised of C_5F_{14} and C_6F_{16} emissions, but no *c*-C_4F_8. *c*-C_4F_8 emissions from category 2E can be estimated using purchased amounts of *c*-C_4F_8 from the NIR and IPCC emission estimation methods (IPCC, 2006) and are likely at most a few t yr^{-1}. If all of Japan's emissions from category 2B9 (fugitive emissions from fluorochemical production) were *c*-C_4F_8, this could equate to several tens to two hundred t yr^{-1}. However, more likely is that the PFC emissions from category 2B9 are due to fugitive emissions from PFC production in Japan, and that their mix is similar to the PFC mix used in Japan for the electronics industries (2E) of CF_4, C_2F_6, C_3F_8, and *c*-C_4F_8. As detailed in the NIR, *c*-C_4F_8 used in category 2E represents 0–7 % of the total PFC mix (CO_2-eq.), which would equate to a few t yr^{-1} from category 2B9. The Netherlands also lists unspecified PFC mix emissions from category 2B9. If we assume a similar mix as for Japan, this would contribute less than 0.6 t yr^{-1} of *c*-C_4F_8.

Two countries report emissions of an unspecified mix of HFCs and PFCs and other fluorinated compounds to the UNFCCC, the United States of America (293 (1990) – 9449 (2014) Gg CO_2-eq.) and Germany (152 (2014) – 5773 (1995) Gg CO_2-eq.). The German NIR details that their emissions of unspecified mix of PFCs and HFCs and other

fluorinated compounds is comprised of various HFCs, hydrofluoroethers (HFE), C_3F_8, higher PFCs, perfluorinated polyether (PFPE), anesthetics, and SF_6 from categories 2B9 and 2H3 (Others), but not *c*-C_4F_8.

The US reports *c*-C_4F_8 emissions of a few t yr^{-1} from category 2E1 (IC or SC production). The NIR details that the US emissions of unspecified mix of PFCs and HFCs and other fluorinated compounds stems from category 2F6 (product uses as substitutes of ozone depleting substances (ODSs), other applications). From the description of category 2F and subcategory 2F6 it seems likely that *c*-C_4F_8 is at most a minor component of category 2F6 which is comprised of various HFCs, HFOs, C_4F_{10}, and a diverse collection of PFCs and PFPEs employed for solvent applications. Based on this one may conclude that no additional *c*-C_4F_8 emissions occur. However, data from the US EPA (https://www.epa.gov/sites/production/files/2018-10/ghgrp_i_freq_request_data_8_19_2018.xlsx, accessed Jan 2019) details that *c*-C_4F_8 emissions from three fluorochemical production facilities in the eastern US ranged from 29 to 62 t yr^{-1} from 2011 to 2017. At least two of these facilities are known to produce TFE, HFP, and/or PTFE and it is likely that these facilities use the process via pyrolysis of HCFC-22, with *c*-C_4F_8 as an intermediate/by-product, which probably is the source of these reported emissions. These *c*-C_4F_8 emissions, which are ~8 times larger than the emissions listed *c*-C_4F_8 emissions from category 2E, are currently not reported in category 2B9 (fluorochemical production). The US EPA intends to report these emissions once emissions for the years 1990 to 2010 have been estimated (currently only data from 2011 onward exists) to fulfil UNFCCC reporting requirements to estimate emissions for each year since 1990 (US EPA, personal communication). It is unclear if these *c*-C_4F_8 emissions are currently reported in the unspecified mix of PFCs and HFCs and other fluorinated compounds.

In summary, data submitted to UNFCCC probably represent 10–30 t yr^{-1} (0.01–0.03 Gg yr^{-1}) of *c*-C_4F_8 emissions, with 25–30 t yr^{-1} (0.025–0.030 Gg yr^{-1}) from 2011 to 2014. After adding the US emissions from fluorochemical production listed by the US EPA, this increases substantially to 50–83 t yr^{-1} (0.05–0.083 Gg yr^{-1}) from 2011 to 2014. It seems that large uncertainties remain due to difficulties disentangling the emissions of unspecified mixes of PFCs and mixes of HFCs/PFCs/other fluorinated compounds and perhaps unquantified or unaccounted for emissions.

The Emissions Database for Global Atmospheric Research (EDGAR) aims to estimate global emissions, including from countries not reporting to the UNFCCC, most notably China, South Korea, and Taiwan which may have significant *c*-C_4F_8 emissions from their electronics and PTFE industries. EDGAR v4.2 (EDGAR, 2010) estimates global *c*-C_4F_8 emission from three sources (SC production, solvent use, fire extinguisher use), but only until 2010. From 1970 to 1985, EDGAR reports no *c*-C_4F_8 emissions, followed by a rise to a few t yr^{-1} in the early 1990s and to ~25 t yr^{-1} (~0.025 Gg yr^{-1}) in 2008, followed by a decline to ~20 t yr^{-1} (0.02 Gg yr^{-1}) in 2010.

For Japan, *c*-C_4F_8 emissions reported by EDGAR are broadly consistent with those calculated from the UNFCCC NIR (see above) from the electronics industry alone (category 2E, assuming an increasing fraction of abatement from 2005 forward); therefore the potential emissions from category 2B9 (fugitive emissions from fluorochemical production) estimated above do not seem to be included in EDGAR.

For South Korea a NIR with data until 2013 can also be obtained (http://www.gir.go.kr/eng/). EDGAR *c*-C_4F_8 emission estimates are broadly consistent with those estimated from the South Korean NIR using IPCC methodologies for the electronics industries (category 2E), a few t yr^{-1} until 2010.

For Taiwan we received *c*-C_4F_8 emissions from their NIR (Chang-Feng Ou-Yang, personal communications). Emissions reported by EDGAR are consistently lower than given in the NIR, at most a t yr^{-1} versus a few t yr^{-1} (since

2001) to ~20 t yr^{-1} (2014). The Taiwanese NIR only includes emissions from SC, IC, and memory production, potentially excluding other emission sources, such as from LCD/TFT production. For China, Malaysia, and Singapore, EDGAR lists only very small emissions of less than a t yr^{-1}. Particularly for China this seems unlikely due to its large electronics and PTFE industries, potential *c*-C_4F_8 sources.

The World Semiconductor Council (WSC) estimates PFC emissions from their member industries in China, Taiwan, Europe, Japan, South Korea, United States, which range from 14 t yr^{-1} in 2012 to 24 t yr^{-1} in 2016.

Based on the available information discussed above we constructed a bottom-up inventory. First, we added for each year and each country emissions reported to UNFCCC and the estimated portion from unspecified mix of PFCs. For 2011 to 2014 we also added the U.S. emissions from fluorocarbon production reported by US EPA. Then we calculated the maximum for each year and each country from these augmented UNFCCC data, US EPA, EDGAR, and estimates from the NIRs, as detailed above. Globally these add up to 10–30 t yr^{-1} (0.01–0.03 Gg yr^{-1}) from 1990 to 1999, 30–40 t yr^{-1} (0.03–0.04 Gg yr^{-1}) from 2000 to 2010, and 100–116 t yr^{-1} (~0.1 Gg yr^{-1}) from 2011 to 2014 (with a substantial fraction due to the U.S. emissions from fluorocarbon production reported by US EPA). WSC emissions discussed above corresponds to ~16 % of these global emissions for the years 2012 to 2014.

Details on the tuning of the CSIRO firn model for the Summit13 site

We use firn air data for 11 tracers from the Summit13, Greenland site (CO_2, CH_4, N_2O, SF_6, CFC-11, CFC-12, CFC-113, CH_3CCl_3, HFC-134a, HCFC-141b, and HCFC-142b), to calibrate the diffusivity-depth profile and other diffusivity-related parameters in the CSIRO firn model using established methods. The firn model includes molecular diffusion throughout the firn (Schwander et al., 1993), and dispersion in the lock-in zone (Buizert and Severinghaus, 2016). The model gives the best match to observations with dispersion in the lock-in zone peaking at around 0.1 m^2 yr^{-1}, consistent with Buizert et al. (2013) and Buizert and Severinghaus (2016), although there were also cases within the 68 % confidence interval that had no lock-in zone dispersion. We tested the use of eddy diffusion for convective mixing near the surface, but the best fit to observations was obtained without is, so it was not used in the final calibration. A melt layer was observed at Summit, due to melting that occurred in July 2012. The melt layer corresponds to a depth of around 60 cm but there were extensive percolated melt features down to around 1.5 m. The melt layer was included in the CSIRO firn model as described in Trudinger et al. (2013). Model layers in the CSIRO firn model move with the ice, and the timing of model layer generation at the surface was chosen so that the influence of the melt layer began in July 2012, and extended down to a model layer boundary that reached around 1.4 m at the time of firn sampling. The model produced the best fit to observations with reduction of diffusion by the melt layer of around 90 % (this value depends on the location of the model layers with time). We generated an ensemble of diffusivity parameters corresponding to a 68 % confidence interval as described in Trudinger et al. (2013), to use this to incorporate firn model uncertainty into the inversion.

Figure S1 shows the optimized diffusivity-depth profile and the modelled depth profiles for the calibration tracers. The atmospheric histories used to force the firn model were those compiled in Buizert et al. (2012) (based on Martinerie et al., 2009) for most tracers for calibration of firn models for the NEEM site, with extension to 2013 using in situ measurements from either Summit in the NOAA network (for CO_2 and CH_4) or Mace Head in the AGAGE network, with correction between the calibration scales used by NOAA and AGAGE where required. For

N_2O, we used the NOAA record at Summit, extended prior to 1998 based on the Law Dome (SH) ice core record (Rubino et al., 2019) and the reconstruction by Prokopiou et al. (2017). For HCFC-141b and HCFC-142b, we compiled atmospheric histories using measurements from Mace Head from late 1994, and extrapolated back to zero before this. Due to the lack of information on atmospheric histories of these HCFCs before 1994, the deepest few measurements of these tracers were not used for calibration (indicated by the grey symbols in Fig. S1). We used larger uncertainties for N_2O measurements prior to the in situ record due to the higher uncertainty in the atmospheric record. We excluded the deep CO_2 measurements from calibration, because at another NH site, NEEM, all models in the firn model intercomparison by Buizert et al., 2012 significantly underestimated CO_2 in the deep firn; the reason for this is not currently understood but could be due to in situ production or fractionation as discussed by Buizert et al. $\delta^{15}N_2$ is shown in Figure S1 but was not used for calibration because it is very sensitive to thermal effects at Summit that are not included in the firn model and not important for *c*-C_4F_8.

Buizert, C., Martinerie, P., Petrenko, V. V., Severinghaus, J. P., Trudinger, C. M., Witrant, E., Rosen, J. L., Orsi, A. J., Rubino, M., Etheridge, D. M., Steele, L. P., Hogan, C., Laube, J. C., Sturges, W. T., Levchenko, V. A., Smith, A. M., Levin, I., Conway, T. J., Dlugokencky, E. J., Lang, P. M., Kawamura, K., Jenk, T. M., White, J. W. C., Sowers, T., Schwander, J., and Blunier, T.: Gas transport in firn: multiple-tracer characterisation and model intercomparison for NEEM, Northern Greenland, Atmos. Chem. Phys., 12, 9, 4259-4277, 10.5194/acp-12-4259-2012, 2012.

Buizert, C., Sowers, T., and Blunier, T.: Assessment of diffusive isotopic fractionation in polar firn, and application to ice core trace gas records, Earth Planet. Sci. Lett., 361, 110-119, 10.1016/j.epsl.2012.11.039, 2013.

Buizert, C., and Severinghaus, J. P.: Dispersion in deep polar firn driven by synoptic-scale surface pressure variability, The Cryosphere, 10, 5, 2099-2111, 10.5194/tc-10-2099-2016, 2016.

Martinerie, P., Nourtier-Mazauric, E., Barnola, J.-M., Sturges, W. T., Worton, D. R., Atlas, E., Gohar, L. K., Shine, K. P., and Brasseur, G. P.: Long-lived halocarbon trends and budgets from atmospheric chemistry modelling constrained with measurements in polar firn, Atmos. Chem. Phys., 9, 12, 3911-3934, DOI 10.5194/acp-9-3911-2009, 2009.

Prokopiou, M., Martinerie, P., Sapart, C. J., Witrant, E., Monteil, G., Ishijima, K., Bernard, S., Kaiser, J., Levin, I., Blunier, T., Etheridge, D., Dlugokencky, E., van de Wal, R. S. W., and Röckmann, T.: Constraining N2O emissions since 1940 using firn air isotope measurements in both hemispheres, Atmos. Chem. Phys., 17, 7, 4539-4564, 10.5194/acp-17-4539-2017, 2017.

Rubino, M., Etheridge, D. M., Thornton, D. P., Howden, R., Allison, C. E., Francey, R. J., Langenfelds, R. L., Steele, P. L., Trudinger, C. M., Spencer, D. A., Curran, M. A. J., Van Ommen, T. D., and Smith, A. M.: Revised records of atmospheric trace gases CO_2, CH_4, N_2O and $\delta^{13}CO_2$ over the last 2000 years from Law Dome, Antarctica, Earth Syst. Sci. Data Discuss., 2018, 1-30, 10.5194/essd-2018-146, 2018.

Schwander, J., Barnola, J. M., Andrie, C., Leuenberger, M., Ludin, A., Raynaud, D., and Stauffer, B.: The Age of the Air in the Firn and the Ice at Summit, Greenland, J. Geophys. Res., 98, D2, 2831-2838, 1993.

Trudinger, C. M., Enting, I. G., Rayner, P. J., Etheridge, D. M., Buizert, C., Rubino, M., Krummel, P. B., and Blunier, T.: How well do different tracers constrain the firn diffusivity profile?, Atmos. Chem. Phys., 13, 3, 1485-1510, 10.5194/acp-13-1485-2013, 2013.

Details on the production of HFO-1234yf from HCFC-22 with potential *c*-C_4F_8 by-product emissions

The hydrofluoroolefin HFO-1234yf ($CF_3CF=CH_2$) is a fourth generation refrigerant replacing HFC-134a in mobile air conditioning (MAC) (Vollmer et al., 2015). It can be produced starting out with similar chemistry that is used for the production of PTFE/FEP, that is the pyrolysis of HCFC-22 to TFE and HFP (Lim et al., 2017), with *c*-C_4F_8 as a by-product that may be vented to the atmosphere. Even though this route to produce HFO-1234yf is not continuous, requiring several batch operations, it is the preferred route in China and India due to the existing large scale HCFC-22, TFE, and HFP production capacities. Honeywell has licensed Navin Fluorine International (NFIL, Surat, Gujarat, India) in 2016 to produce HFO-1234yf (www.coolingpost.com/world-news/honeywell-licences-r1234yf-production-in-india, accessed 2019/07/01). This facility is one of the PTFE producing facilities shown in Fig. 9 in Western India. Honeywell has also licensed the Juhua Group Corporation in China in 2016 to produce HFO-1234yf (www.springerprofessional.de/betriebsstoffe/honeywell-laesst-1234yf-auch-in-china-produzieren/10062482, accessed 2019/07/01, German, translate.google.com). The likely location of this HFC-1234yf production in China corresponds to one or both of to the two Juhua Group Corporation PTFE production facility shown in Fig. 7 in Zhejiang province. Other facilities licensed by Honeywell to produce HFO-1234yf using this route with potential *c*-C_4F_8 emissions may exist in East Asia, but any such production is relatively recent and cannot explain historic *c*-C_4F_8 emissions.

Lim, S., Kim, M. S., Choi, J.-W., Kim, H., Ahn, B. S., Lee, S. D., Lee, H., Kim, C. S., Suh, D. J., Ha, J.-M., and Song, K. H.: Catalytic dehydrofluorination of 1,1,1,2,3-pentafluoropropane (HFC-245eb) to 2,3,3,3-tetrafluoropropene (HFO-1234yf) using in-situ fluorinated chromium oxyfluoride catalyst, Catalysis Today, 293-294, 42-48, 10.1016/j.cattod.2016.11.017, 2017.

Vollmer, M. K., Reimann, S., Hill, M., and Brunner, D.: First Observations of the Fourth Generation Synthetic Halocarbons HFC-1234yf, HFC-1234ze(E), and HCFC-1233zd(E) in the Atmosphere, Environ. Sci. Technol., 49, 5, 2703-2708, 10.1021/es505123x, 2015.

Supplemental Figures

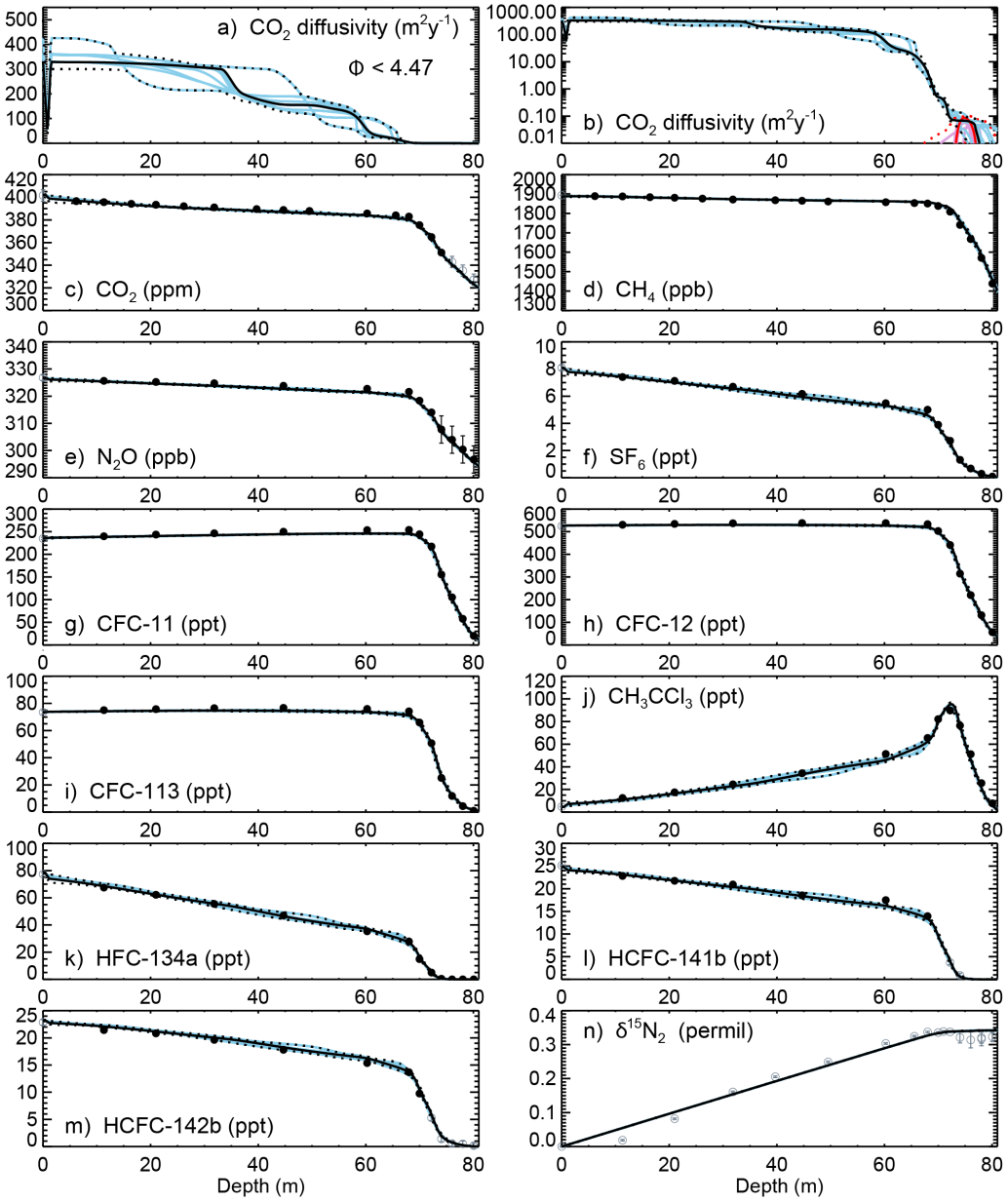

Figure S1. Tuning of the CSIRO firn model for the Summit13 site: CO_2 diffusivity on linear and log scales, and concentration profiles of CO_2, CH_4, N_2O, SF_6, CFC-11, CFC-12, CFC-113, CH_3CCl_3, HFC-134a, HCFC-141b, and HCFC-142b, as well as the $\delta^{15}N_2$ profile. The solid black lines show the case with the closest match to all observations used for diffusivity calibration. The dotted black lines show the upper and lower ranges of all cases that correspond approximately to a 68 % confidence interval. The blue curves show some representative cases within the 68 % confidence interval that are used in the CSIRO inversion to incorporate firn model uncertainty. In a) and b), the black and blue lines show molecular diffusivity, while in b), the red lines show dispersion in the lock-in zone (the red solid line is our best case, red dotted lines correspond to the 68 % confidence interval, and the pink lines show some representative cases). Measurements shown by black circles were used for calibration, and measurements shown by the grey circles were not used (see text).

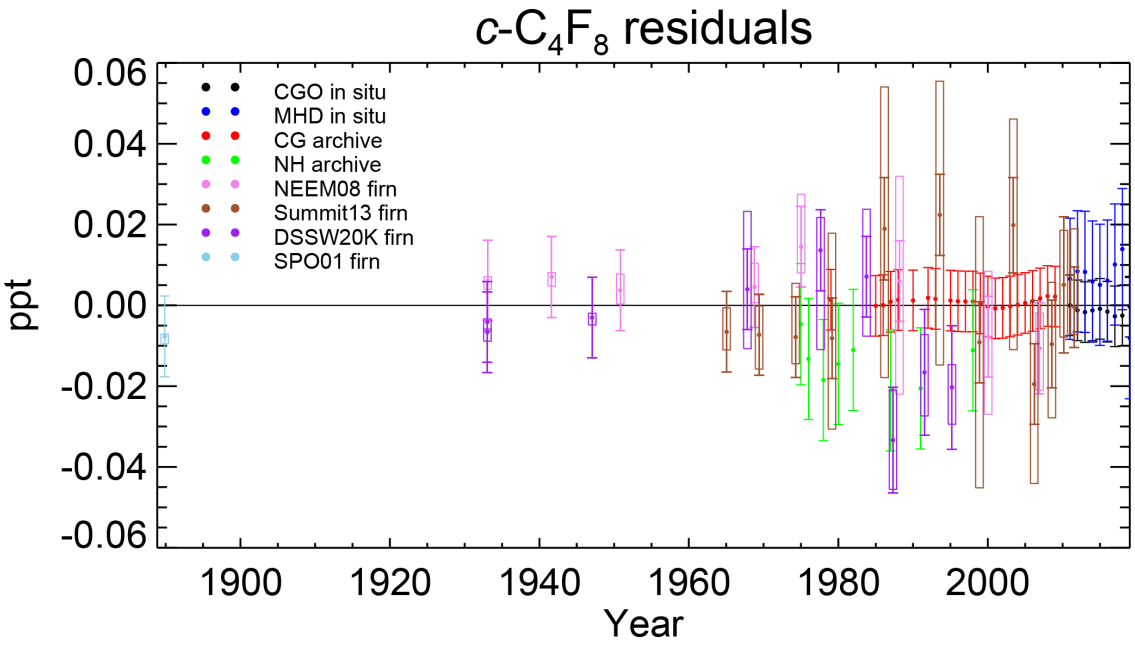

Figure S2. Residuals (model - observations) for the CSIRO inversion based on firn data and annual values from the smoothing spline in each hemisphere to in situ and archive data. The error bars show measurement errors used in the inversion (for the annual values this is the magnitude of correlated errors and for the firn data these are the measurement errors with a lower threshold of 0.01 ppt). The boxes show the range of uncertainties derived from the ensemble of Green's functions from the firn model.

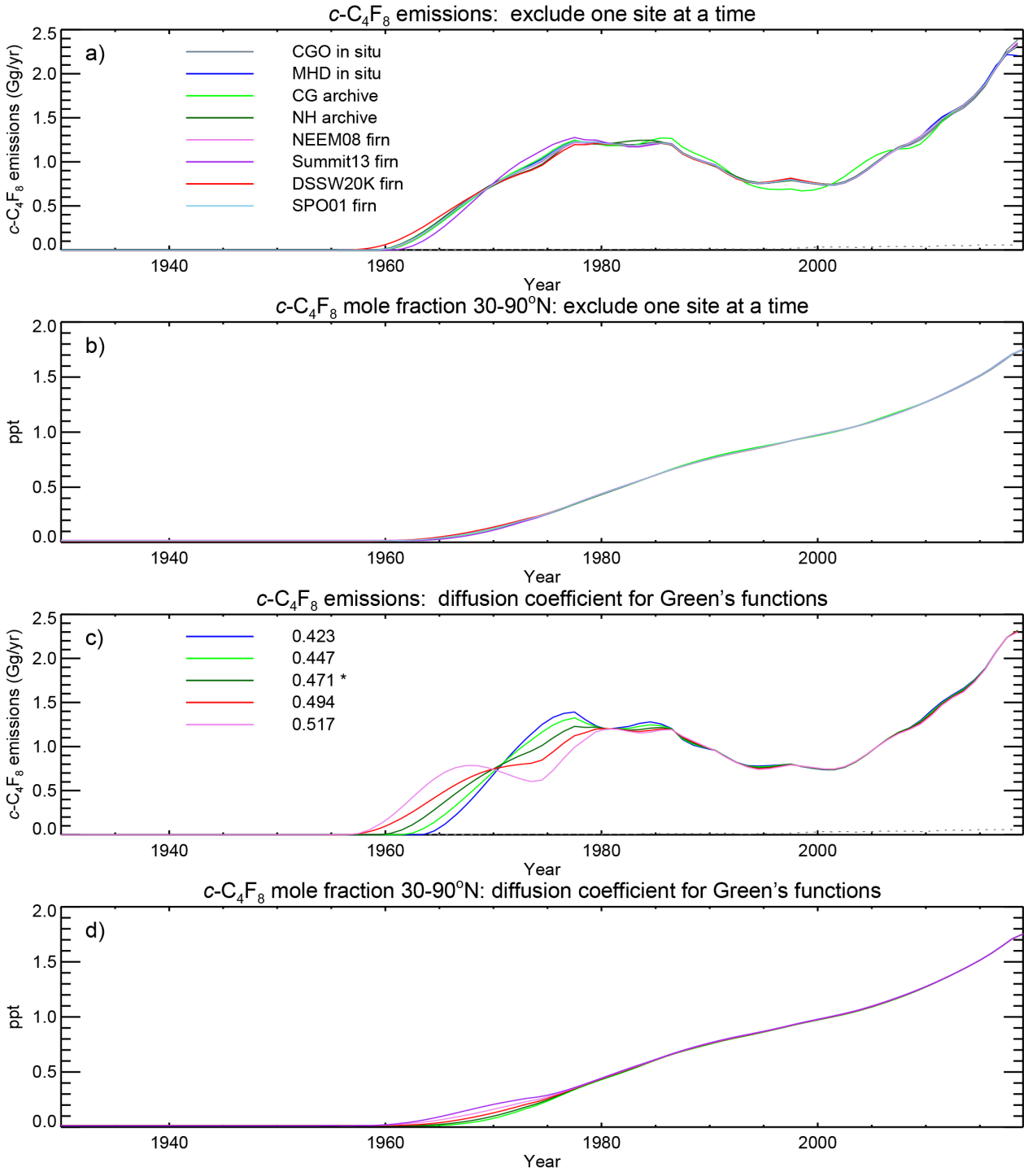

Figure S3. Sensitivity tests with the CSIRO inversion for removal of individual data subsets and uncertainty in the diffusion coefficient: a) inferred emissions with one firn site or in situ or archive part of the atmospheric record in each hemisphere left out at a time; b) same as a but inferred mixing ratios; c) inferred emissions for different values of the diffusion coefficient of *c*-C_4F_8 relative to CO_2, with values from -10 % to +10 %; d) same as c but inferred mixing ratios.

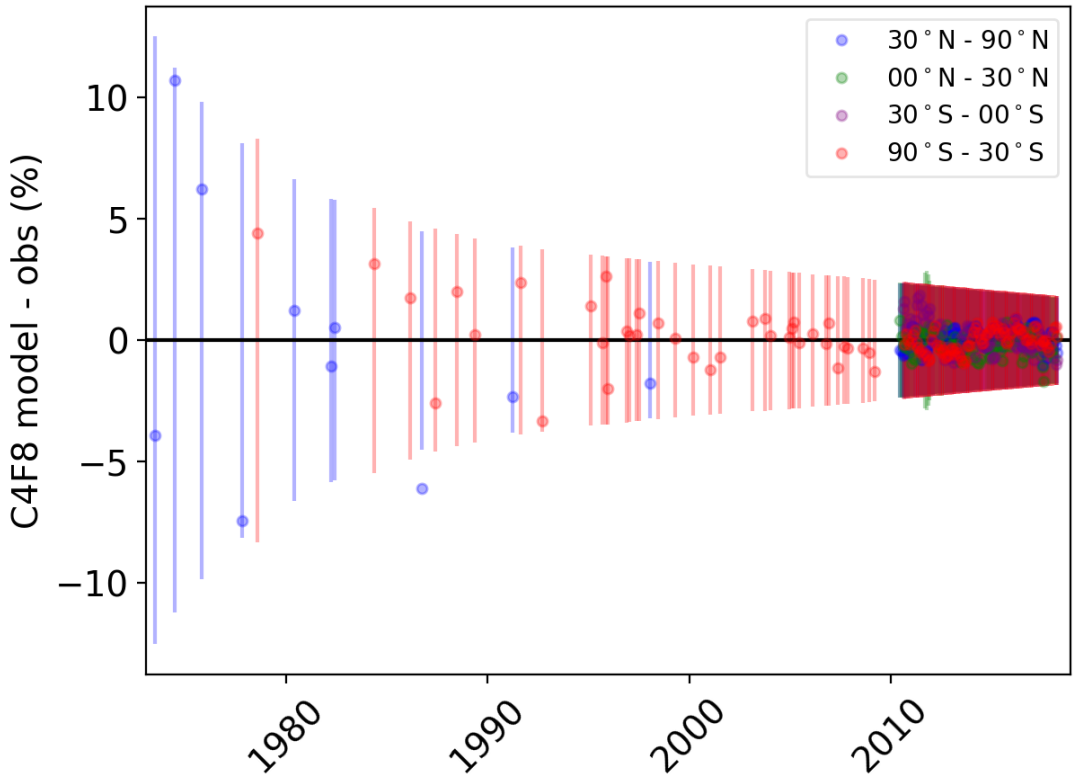

Figure S4. Residuals (model - observations) for the Bristol inversion based on archive and in situ data.

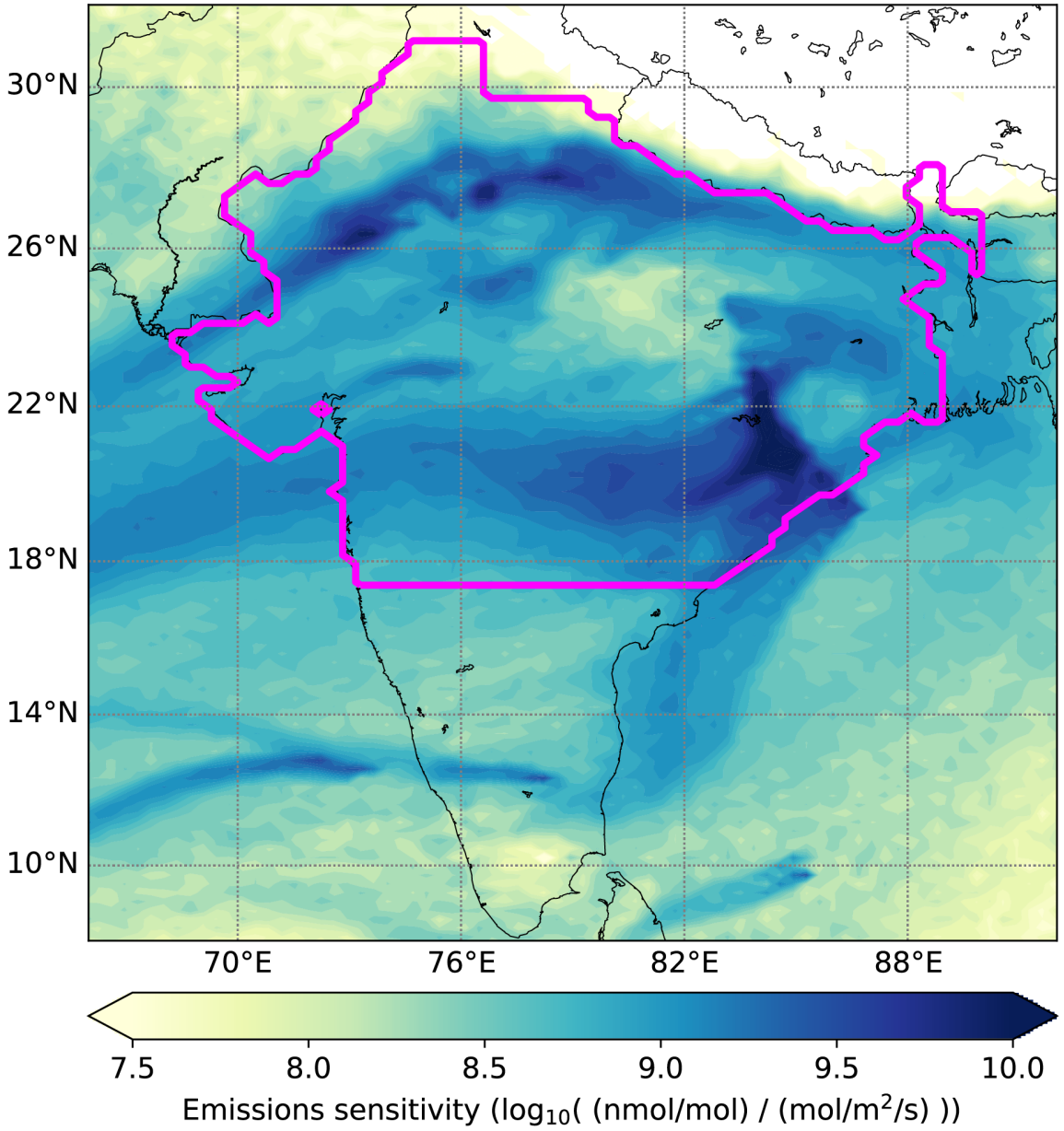

Figure S5. Emissions sensitivity averaged across all measurements made over the Indian subcontinent in June and July 2016. The region roughly corresponding to a maximum in emissions sensitivity is enclosed by the pink line. We denote this region as Northern and Central India (NCI).

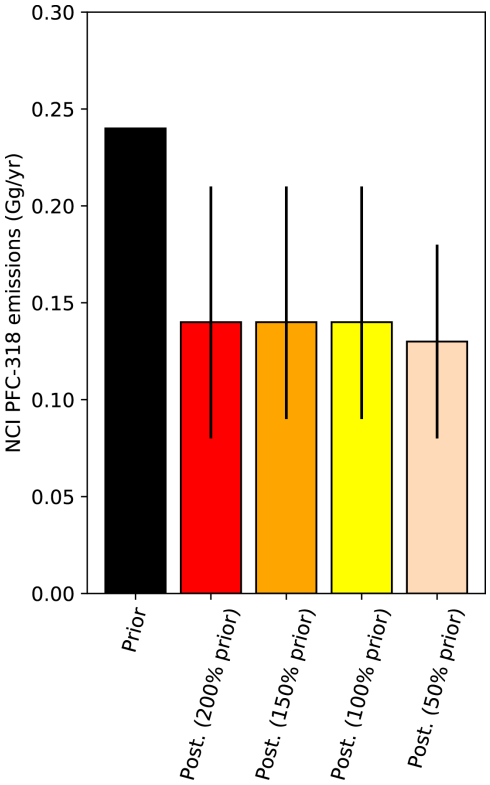

Figure S6. Sensitivity tests for the NAME-HB inversion for the Indian subcontinent. Emissions derived from priors of varying magnitudes (200% of the original prior, red bar, 150% of the original prior, orange bar, and 50% of the original prior, peach bar) indicate that *c*-C_4F_8 emissions determined for Northern and Central India are very insensitive to the choice of prior. The original prior (black bar) and posterior (yellow bar) estimates are also shown. For each estimate, error bars represent the 95% confidence interval of the posterior probability density function.

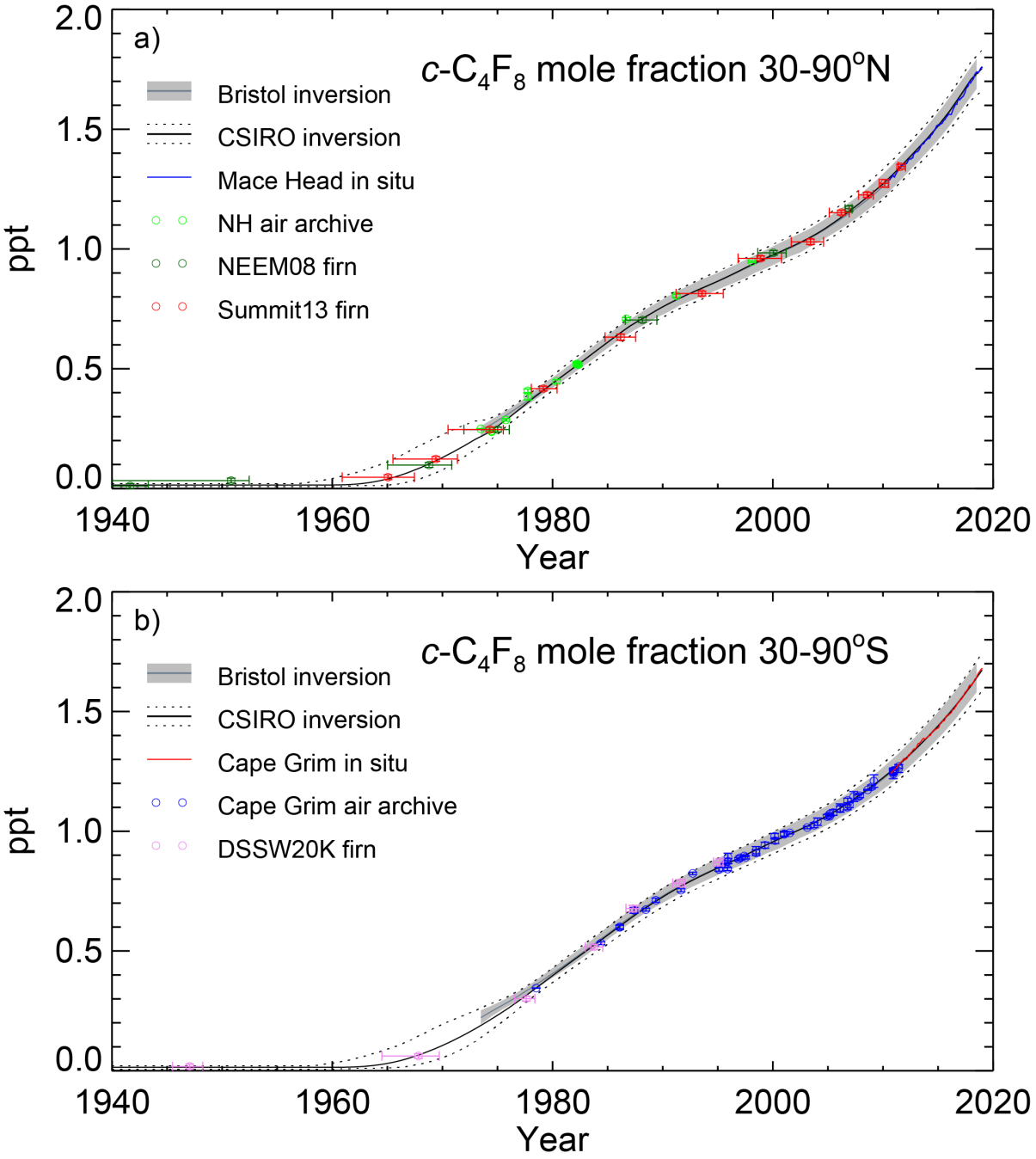

Figure S7. *c*-C_4F_8 extra-tropical mole fractions (ppt) reconstructed by the UB (grey line) and CSIRO (black line) inversions are shown with 2σ uncertainty bands (grey band and black dotted line, respectively) and the underlying in situ (pollution removed monthly means), archive, and firn air data: a) for 30-90°N MHD in situ (blue line), NH archive (light green circles), and the NH firn sites NEEM08 (dark green circles) and Summit13 (red circles); (b) for 30-90°S CGO in situ (red line), the Cape Grim air archive (CGAA, blue circles), and the SH firn site DSSW20K (pink circles); Firn samples are plotted against mean ages (before 1965) or effective ages (after 1965) with 2σ uncertainties as horizontal error bars. Vertical error bars represent precisions for archive and firn data. Uncertainties in monthly means for in situ data have been omitted for clarity (they are shown in Fig. 1).

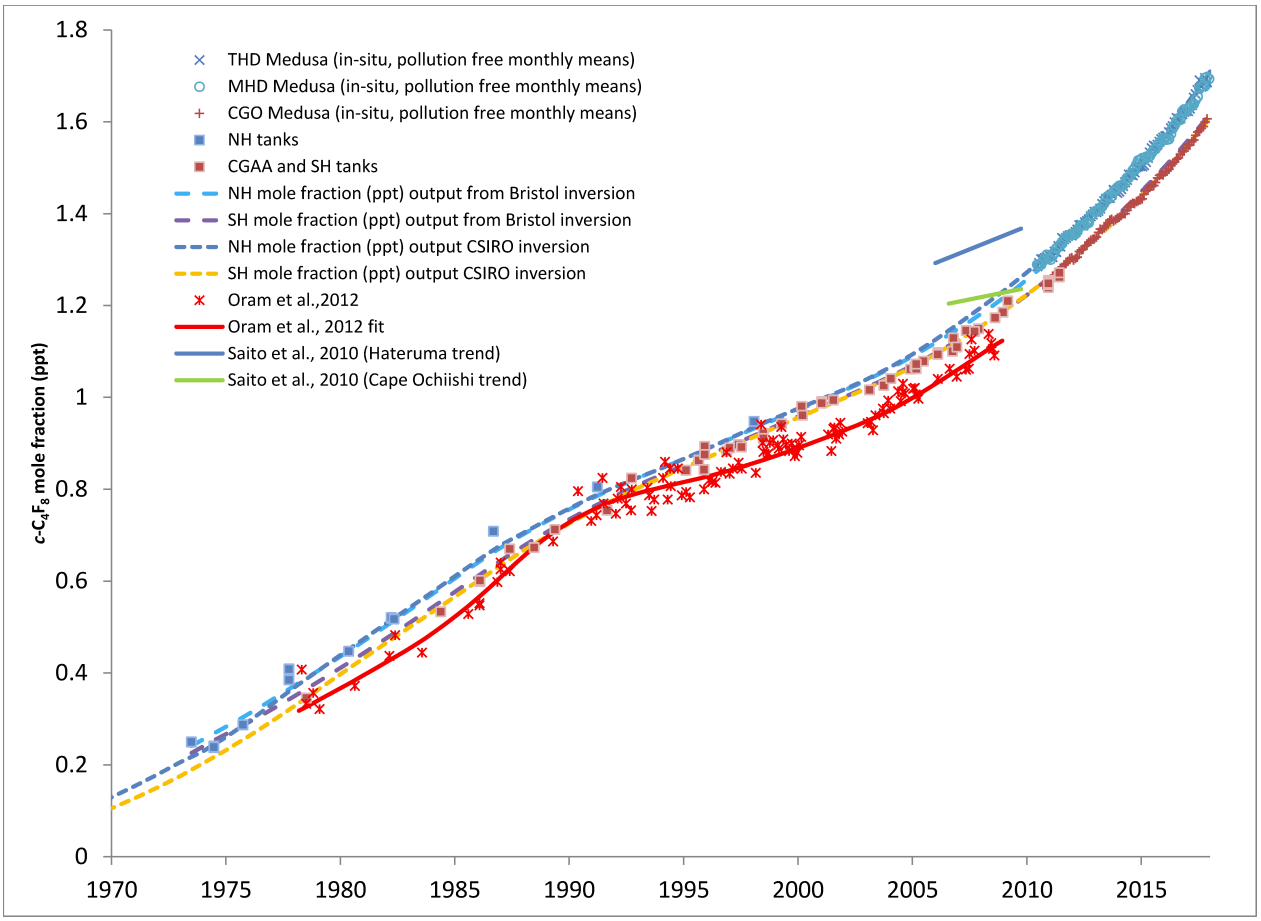

Figure S8. *c*-C_4F_8 mole fractions reconstructed here for the Northern (NH) and Southern Hemisphere (SH) compared to results from Oram et al., 2012 (SH only) and Saito et al., 2010. Measured *c*-C_4F_8 mole fractions from THD, MHD, and CGO Medusa (in situ, pollution-free monthly means, blue crosses and blue circles (NH), red pluses (SH) and NH (blue squares) and CGAA and SH tanks (red squares) are shown together with results from the Bristol (AGAGE 12-box, light blue (NH) and purple (SH) long dashes) and CSIRO (dark blue (NH) and orange (SH) short dashes) inversions. *c*-C_4F_8 mole fractions from Oram et al., 2012 (CGAA/SH only, red stars and red solid line) and Saito et al., 2010 (Hateruma island, blue solid line, Cape Ochiishi, green solid line, both NH) are shown for comparison.

Oram, D. E., Mani, F. S., Laube, J. C., Newland, M. J., Reeves, C. E., Sturges, W. T., Penkett, S. A., Brenninkmeijer, C. A. M., Röckmann, T., and Fraser, P. J.: Long-term tropospheric trend of octafluorocyclobutane (*c*-C_4F_8 or PFC-318), Atmos. Chem. Phys., 12, 1, 261-269, 10.5194/acp-12-261-2012, 2012.

Saito, T., Yokouchi, Y., Stohl, A., Taguchi, S., and Mukai, H.: Large emissions of perfluorocarbons in East Asia deduced from continuous atmospheric measurements, Environ. Sci. Technol., 44, 11, 4089-4095, 10.1021/es1001488, 2010.

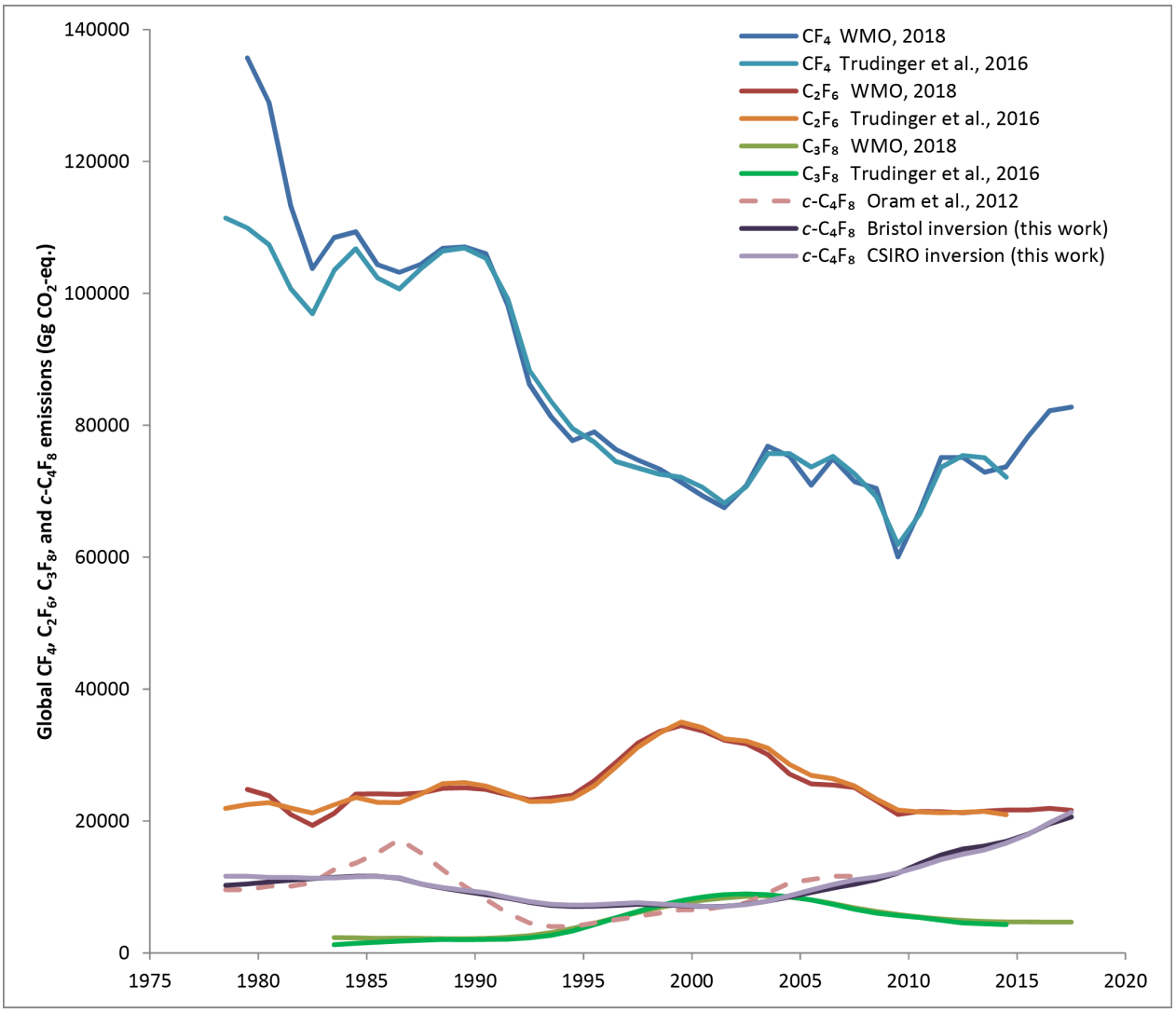

Figure S9. Global emissions of CF_4, C_2F_6, C_3F_8, and *c*-C_4F_8 expressed as carbon dioxide equivalent emissions (CO_2-eq.) emissions (using GWP_{100} of 6,630, 11,100, 8,900, and 9,540, respectively, Burkholder et al., 2018) (1.000.000 Gg CO_2-eq. = 1 billion tonnes CO_2-eq.). In 2017, *c*-C_4F_8 emissions have reached 0.021 billion tonnes of CO_2-equivalent compared to 0.083, 0.022, and 0.005 billion tonnes of CO_2-eq. for CF_4, C_2F_6, and C_3F_8.

Burkholder, J. B. (Lead Author)., Hodnebrog, Ø., and Orkin, V. L. (Contributors).: Appendix A: Summary of Abundances, Lifetimes, Ozone Depletion Potentials (ODPs), Radiative Efficiencies (REs), Global Warming potentials (GWPs), and Global Temperature ChanGe Potentials (GTPs), in: Scientific Assessment of Ozone Depletion: 2018, Global Ozone Research and Monitoring Project–Report No. 58, World Meteorological Organization, Geneva, Switzerland, 2018.

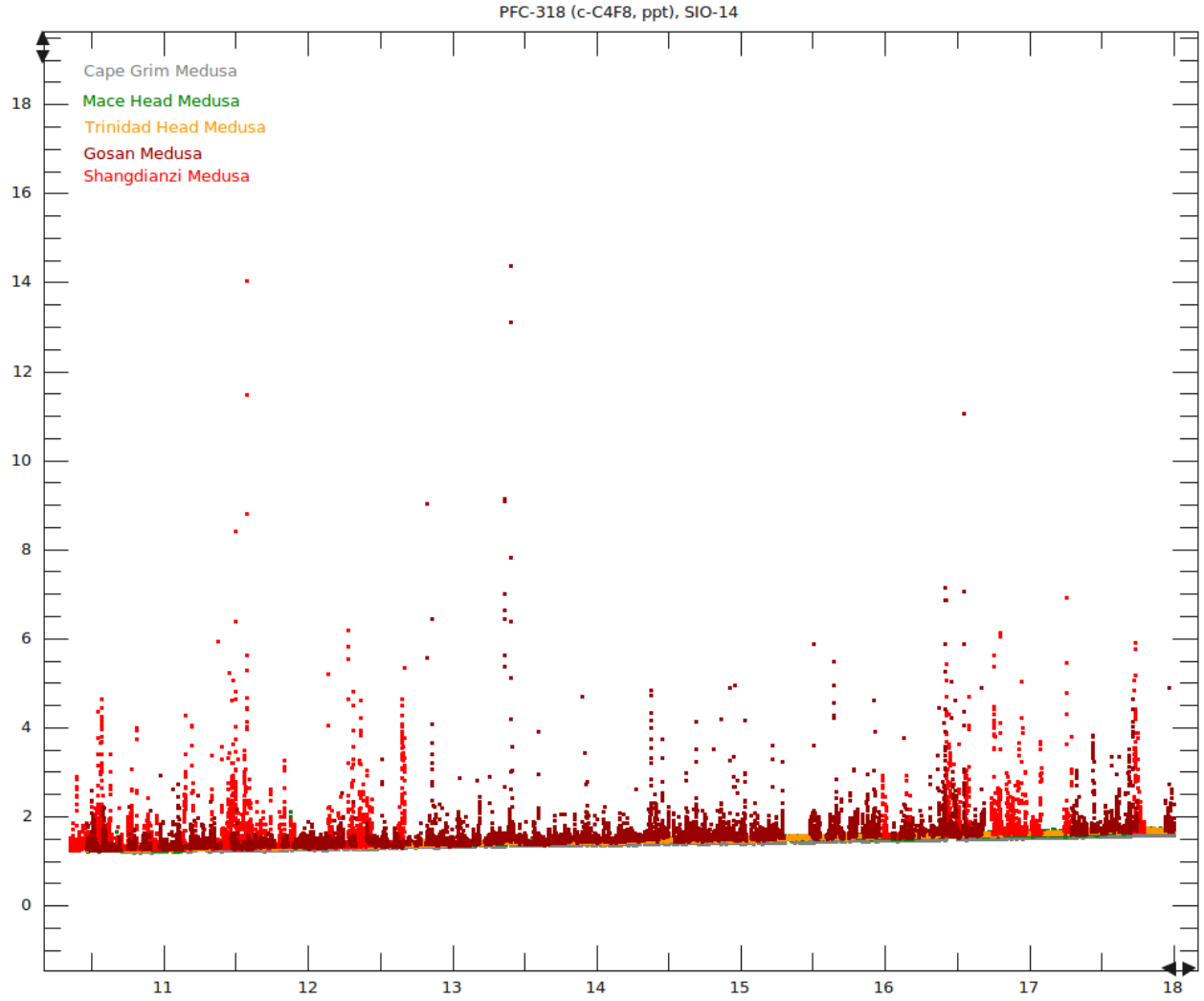

Figure S10. Magnitude of pollution events in East Asia. Among all stations of the AGAGE network, the two stations in eastern Asia, Gosan (brown) and Shangdianzi (red), show by far the most frequent and most pronounced pollution events of up to ~14 ppt above NH background (Mace Head, green, Trinidad Head, orange), indicating significant regional emissions. Measurements at Cape Grim, Australia (light grey), representing SH background, are also shown for comparison.

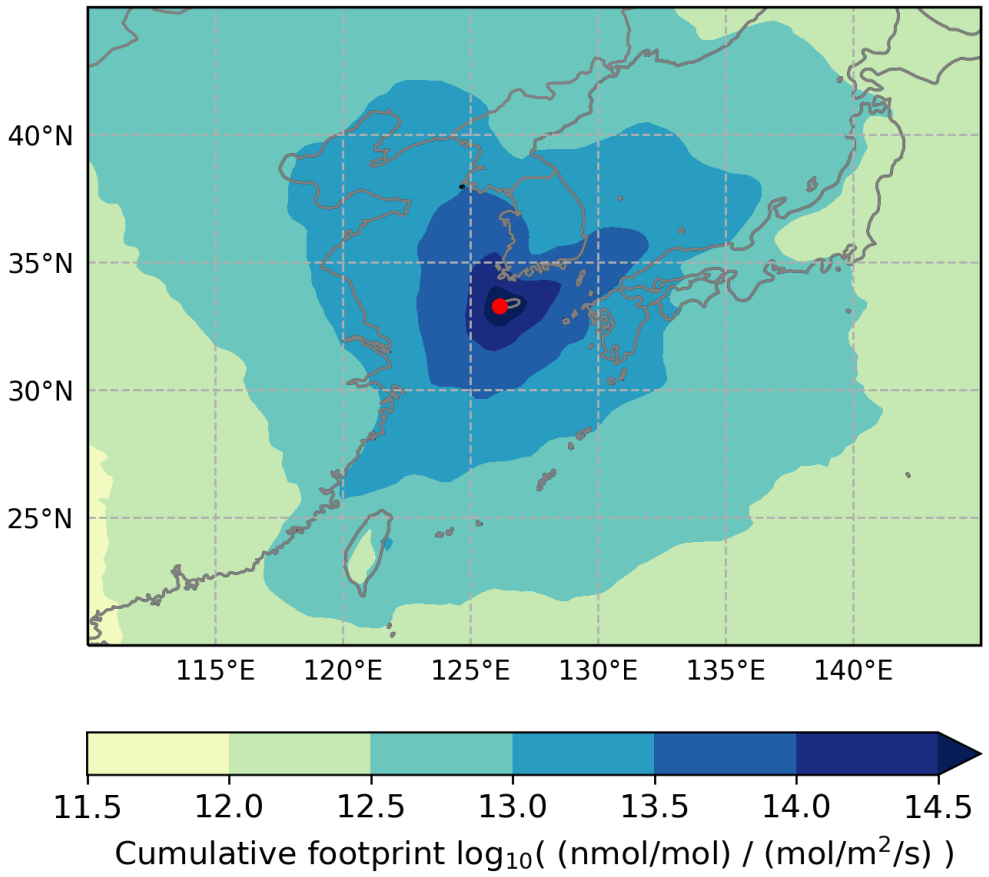

Figure S11. Cumulative footprint map for measurements at Gosan station, Jeju island, South Korea from 2010-2017 generated using the NAME transport model. The footprint indicates where the receptor station is sensitive to emissions. The sensitivity of the inversion generally decreases with distance to the receptor station resulting in relatively low sensitivity for emissions from western China, eastern Japan and Taiwan. Therefore, we report emissions for eastern China, western Japan, South Korea, North Korea, and parts of Taiwan. Eastern China contains the provinces Anhui, Beijing, Hebei, Henan, Jiangsu, Liaoning, Shandong, Shanghai, Shanxi, Tianjin and Zhejiang. Western Japan contains the prefectures Chugoku, Kansai, Shikoku and Okawa and Kyushu.

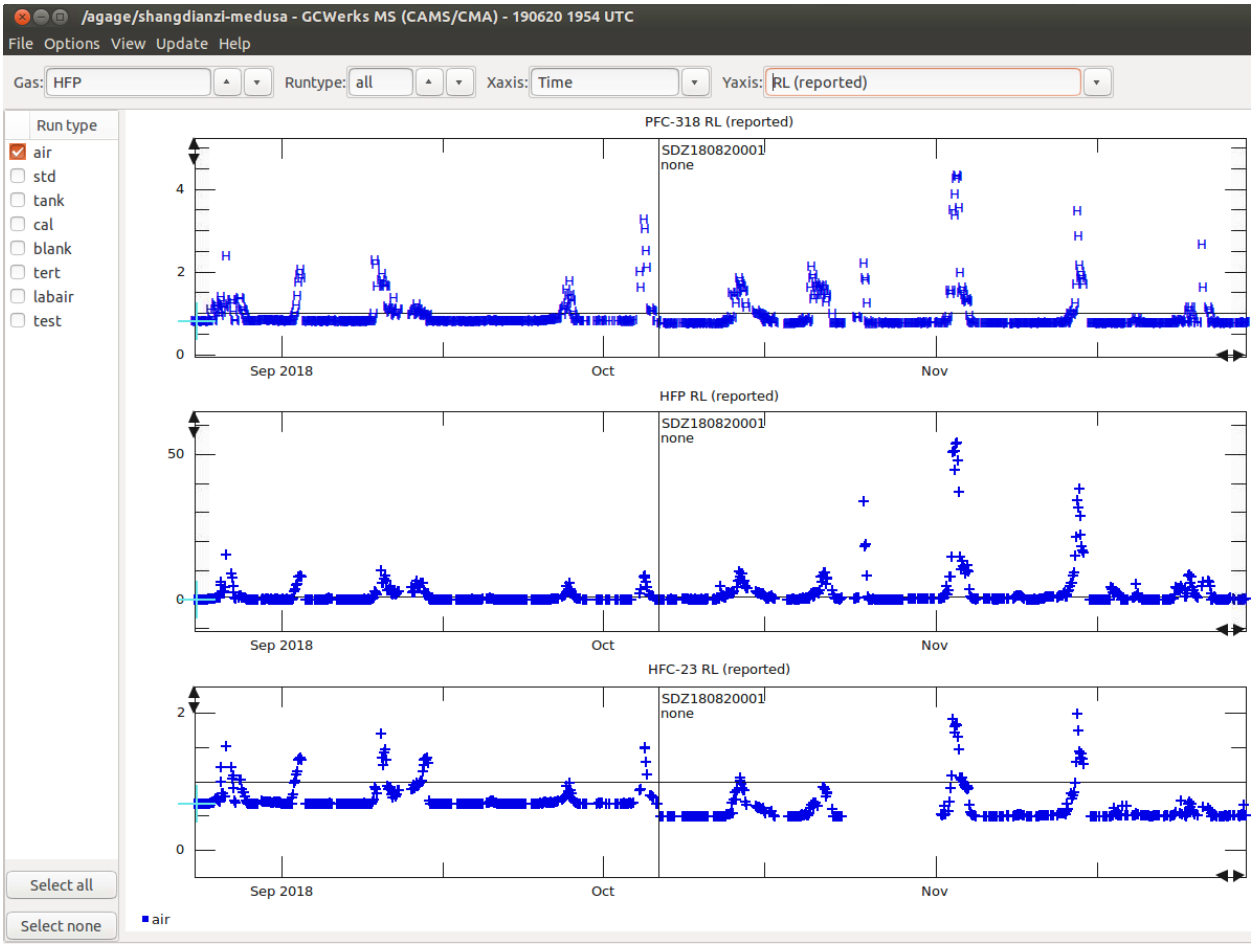

Figure S12. Area responses of ambient air samples relative to those of the working standard (RL (reported)) for *c*-C_4F_8 (PFC-318), HFP (hexafluoropropylene), and HFC-23 measurements at SDZ.

HFP (hexafluoropropylene) is measured on m/z 131 and 150. On the Porabond Q column it elutes after HFC-125 and before CFC-115. We confirmed its identify with a spike of ~10 ppt HFP (87,422 area counts) at SIO. The working standard used at the time contained ~0.03–0.04 ppt HFP (270–380 area counts). Ambient air samples contained ~0.01 ppt HFP (98–123 area counts), just around estimated detection limit of ~0.01 ppt (3 times baseline noise). The low abundance in the working standards led to poor precisions of ~20%. From Nov. 2018 until present, ambient air at SIO typically showed 0–0.5 times (0–150 area counts) the response of the working standard used (reaching a few times to 2.5 times), indicating continuing miniscule ambient mixing ratios. HFP measurements at Aspendale (ASA) have not been calibrated, but the peak responses in ambient air from Feb. 2017 until present were almost always small (0–300 area counts), indicating similarly small ambient mixing ratios as at SIO. Occasional small pollution events have been observed at ASA, see Section 5.3.3. HFP measurements at GSN and SDZ were not calibrated, but several working standards showed significant peak responses (up to 2,500 and 4,000 area counts, respectively). From Aug. 2018 until present, HFP pollution events at SDZ always coincided with *c*-C_4F_8 and HFC-23 pollution events. Figure S12 shows examples of the good correlations observed among PFC-318 (*c*-C_4F_8), HFP, and HFC-23.

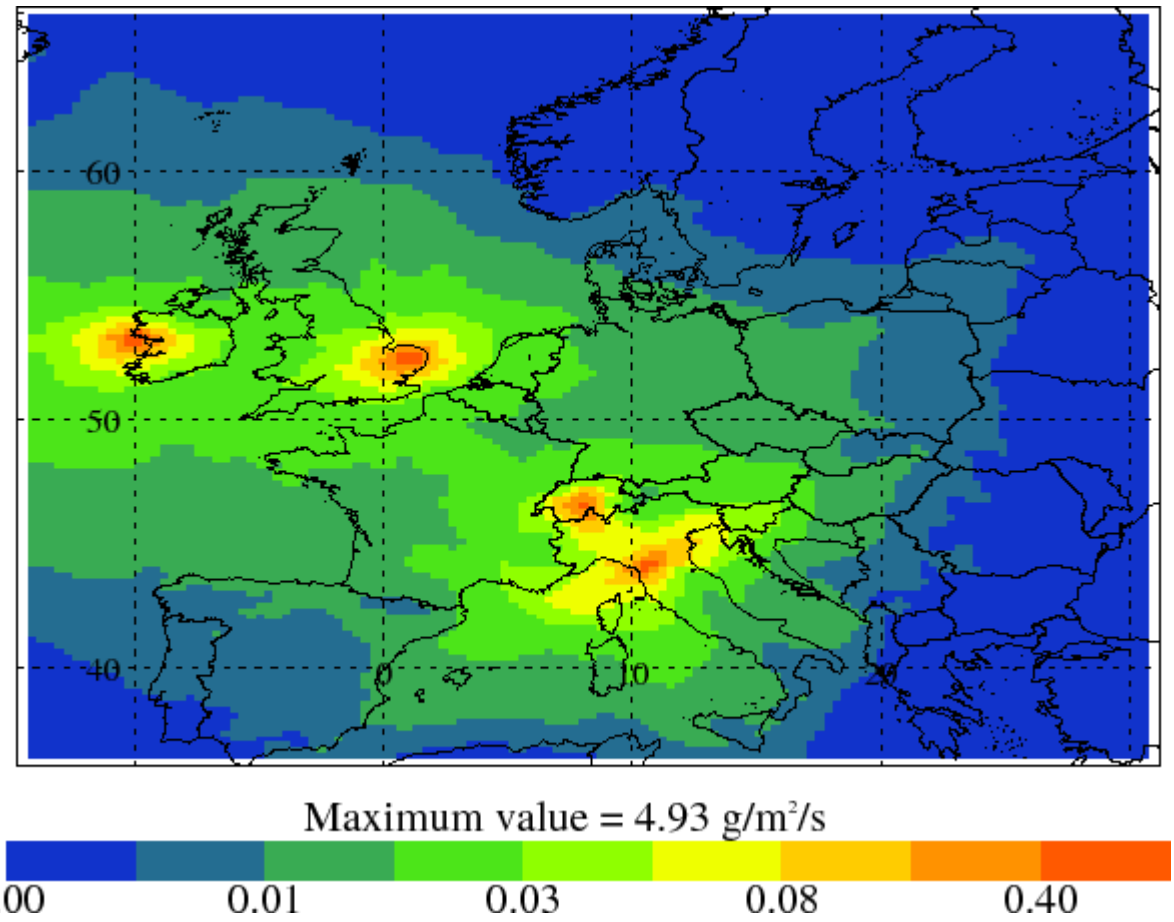

Figure S13: Cumulative footprint map for measurements at the Tacolneston, United Kingdom, Mace Head, Ireland, Jungfraujoch, Switzerland, and Monte Cimone, Italy stations for 2013. The sensitivity of the InTEM inversion is shown in arbitrary units. We report only estimated emissions from North Western Europe (42° N to 59° N and -11° E to 15° E) based on to the areas of highest sensitivity to the observations.

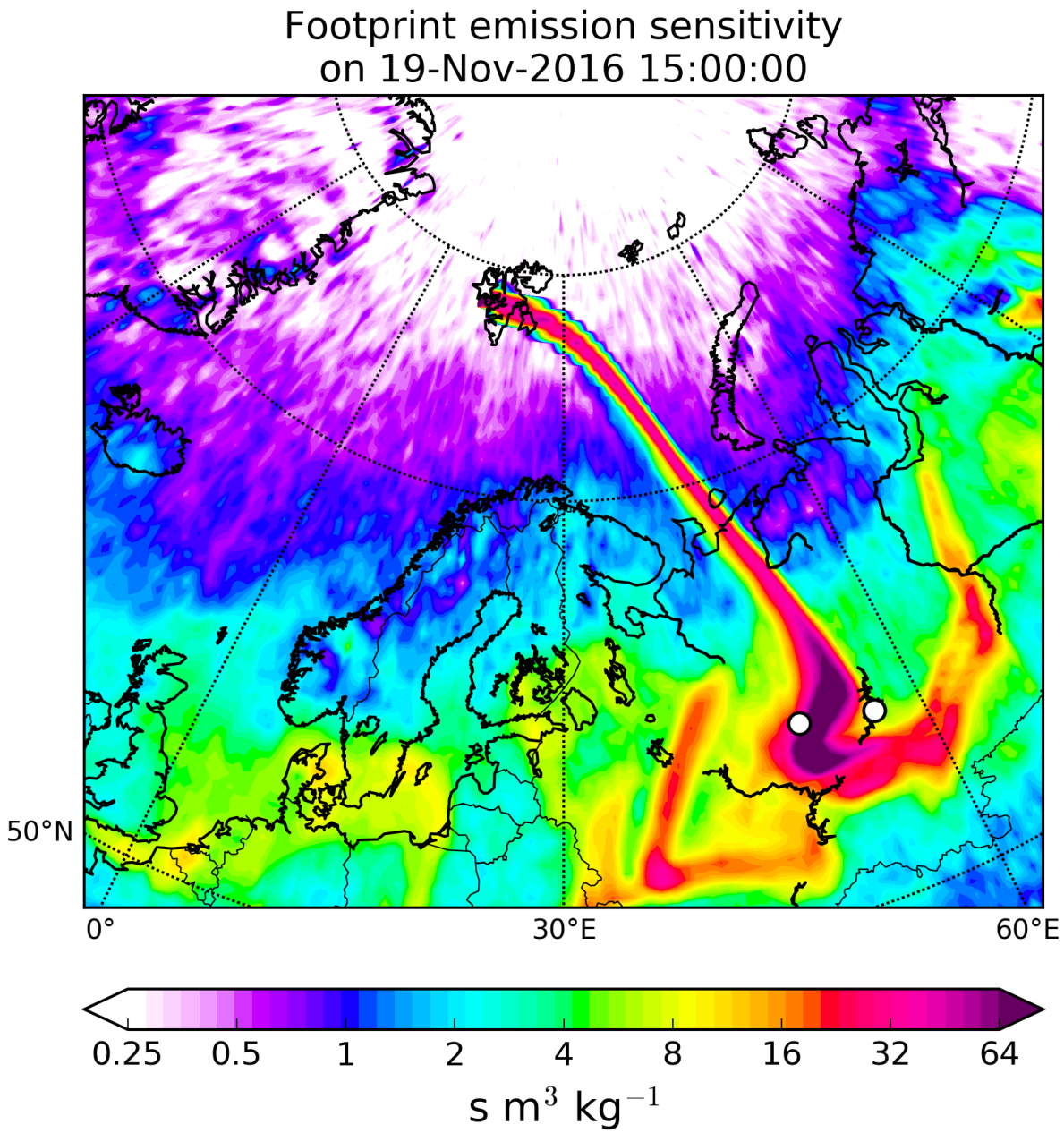

Figure S14. FLEXPART backward simulation for the strong *c*-C_4F_8 pollution event observed at Zeppelin station on November 19, 2016 indicate that this pollution event may be the result of direct transport of air from two facilities which produce PTFE and halogenated chemicals including *c*-C_4F_8 (HaloPolymer, Kirovo-Chepetsk, Kirov Oblast, 58.55° N and 49.99° E and Galogen Open Joint-Stock Company, Perm, Russia, 57.92° N and 56.14° E each site marked with a white dot) to the Zeppelin station (marked with a white star).

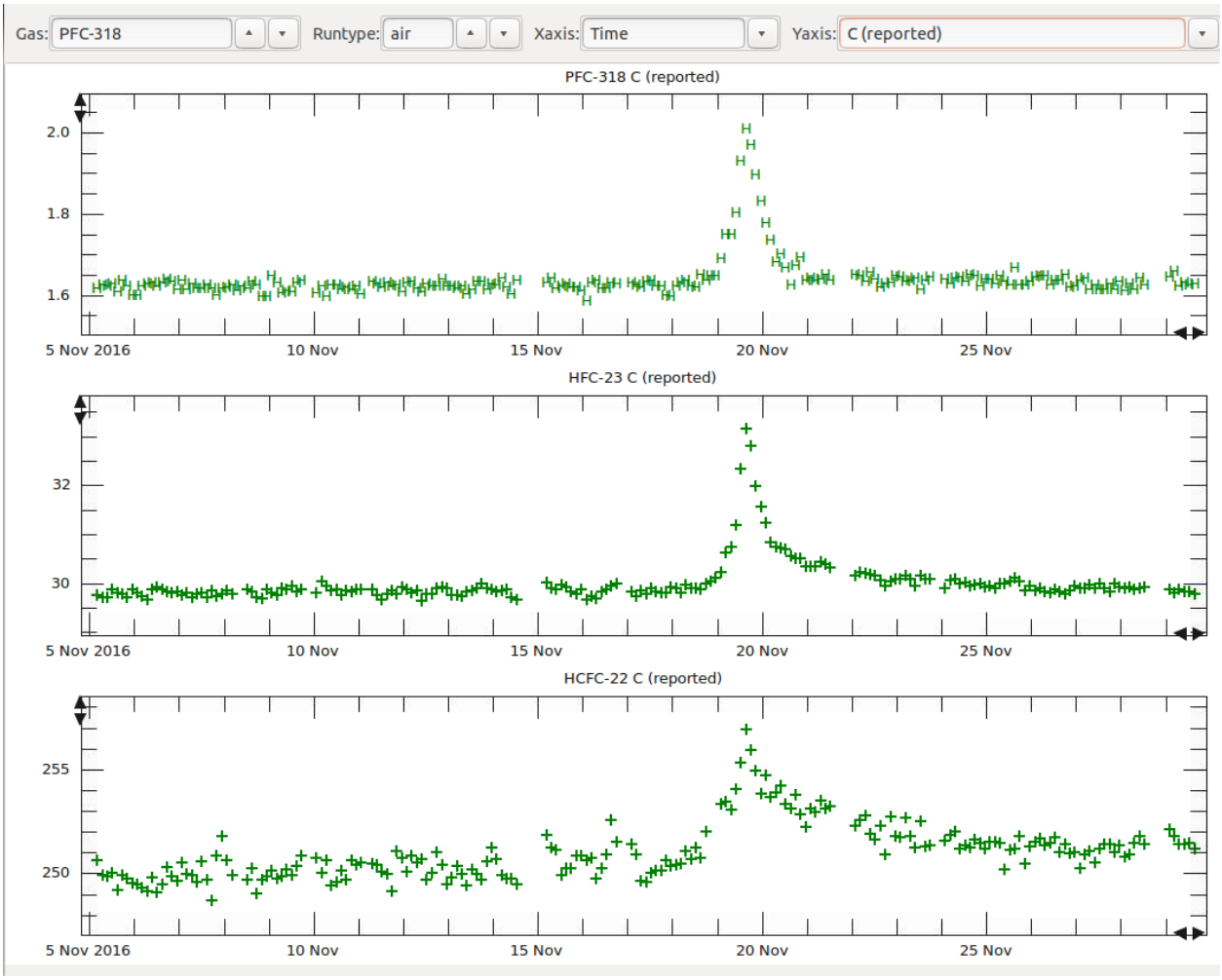

Figure S15. PFC-318 (*c*-C_4F_8), HFC-23, and HCFC-22 mixing ratios in ambient during the largest PFC-318 pollution event at ZEP.

The best correlation was observed between PFC-318 (*c*-C_4F_8) and HFC-23 mixing ratios (C (reported)). Other compounds, such as HCFC-22 (shown above), CFC-13, CH_2Cl_2, $CHCl_3$, or TCE showed weaker correlations. Most other halogenated compounds showed no obvious correlations.

Supplemental Tables

Table S1. The probability distributions assigned to the emissions and boundary conditions scaling and hyperparameters. Fixed parameters are those which have a fixed distribution that remain unchanged during the inversion. Hyperparameters represent the uncertainty in the uncertainties in the statistical model. These variable hyperparameters are estimated with their associated uncertainty within the NAME-HB inversion framework. This uncertainty translates into the total uncertainty in the posterior emissions estimates.

Parameter	Probability distribution	Fixed or variable?
Emissions and boundary conditions scaling	Log-normal(1,10)	Fixed
Model error (ppt)	Uniform(0.1, 10)	Variable
Correlation length scale (hours)	Uniform(1,120)	Variable
Number of Voronoi cells	Uniform(4,200)	Variable

Table S2. Chinese production of PTFE and FEP fluoropolymers (t yr^{-1}) and five year rise rates, including 2015–2020 forecast from the 13th Chinese five year plan

	2000	2005	2010	2011	2014	2015	2020*
PTFE	8,377	26,700	52,078	52,310	91,608	96,335	140,000
FEP			3,865		10,975	12,937	19,000
Fluoropolymers (total)			60,153		122,190	131,320	194,000
PTFE (% total)			87 %		75 %	73 %	72 %
FEP (% total)			6 %		9 %	10 %	10 %
% yr^{-1} increase		2000-2005	2005-2010			2010-2015	2015-2020*
PTFE		26 %	14 %			13 %	7.8 %
FEP						27 %	8.0 %

www.qianzhan.com/analyst/detail/220/170629-c33a2ca7.html, accessed Dec. 2018 (Chinese, translate.google.com)

*Forecast from the 13th Chinese five year plan.

Table S3. Estimates of global PTFE market share by region

	2012[%]	2015[+]	2015[+]	2015[#]	2015[#]
North America	31 %	10 %	10 %	see RoW	
Europe	21 %	14 %	14 %	see RoW	
Asia Pacific (Total)	36 %	62 %		78 %	
China			53 %		67 %
Japan			9 %		11 %
Rest of World (RoW, Total)	12 %	14 %		22 %	22 %
India			8 %		
Russia			6 %		
Total	100 %	100 %	100 %	100 %	100 %

[%]Polytetrafluoroethylene (PTFE), Market Analysis, www.grandviewresearch.com, accessed Oct. 2018.

RoW is comprised of India and Russia.

[+]Polytetrafluoroethylene (PTFE), A Global Market Overview, www.industry-experts.com, accessed Jul. 2018.

RoW is comprised of India and Russia.

[#]www.qianzhan.com/analyst/detail/220/170629-c33a2ca7.html, accessed Dec. 2018 (Chinese, translate.google.com).

RoW is comprised of North America, Europe, India, and Russia.

In 2015, PTFE production in China was estimated to account for 53 - 67% of global PTFE production.

Table S4. Estimates of global PTFE market share by company

	2012[%]		2015[#]
DuPont	31.0 %	Dupont (Global incl. China)	13 %
Daikin	14.0 %	Daikin (Global incl. China)	13 %
Solvay	11.5 %	Solvay (China)	4 %
3M	9.0 %	3M	4 %
Others	31.0 %	Shangdong Dongyue Group	20 %
		Others (China)	30 %
		Others (Global excl. China)	11 %
Arkema SA	5.5 %		
Gujarat Fluorochemicals Ltd.	3.5 %		
		Asahi Glass (Japan)	5 %
Total	100.0 %		100 %

[%]Polytetrafluoroethylene (PTFE), Market Analysis, www.grandviewresearch.com, accessed Oct. 2018

[#]www.qianzhan.com/analyst/detail/220/170629-c33a2ca7.html, accessed Dec. 2018 (Chinese, translate.google.com).

DuPont incl. Chemours, Solvay incl. Solexis, 3M incl. Dyneon, and Asahi Glass incl. AGC.